THE JOURNAL OF PHYSICAL CHEMISTRY B

Article

pubs.acs.org/JPCB

Protein Aggregation: Kinetics versus Thermodynamics

Piero Ricchiuto, Andrey V. Brukhno, and Stefan Auer*

Centre for Molecular Nanoscience, School of Chemistry, University of Leeds, Leeds LS2 9JT, United Kingdom

Supporting Information

ABSTRACT: In this study, we address the questions of how important is the kinetics in protein aggregation, and what are the intrinsic properties of proteins that cause this behavior. On the basis of our recent quantitative calculation of the equilibrium phase diagram of natively folded α-helical and β-sheet forming peptides, we perform molecular dynamics simulations to demonstrate how the aggregation mechanism and end product depend on the temperature, concentration, and starting point in the phase diagram. The results obtained show that there are severe differences between the thermodynamically predicted and the kinetically obtained aggregate structures. The observed differences help to rationalize the suggestion that monomeric proteins in their native functional structure can be metastable with respect to the amyloid state, and that the native fold is a special property that protects them from aggregation.

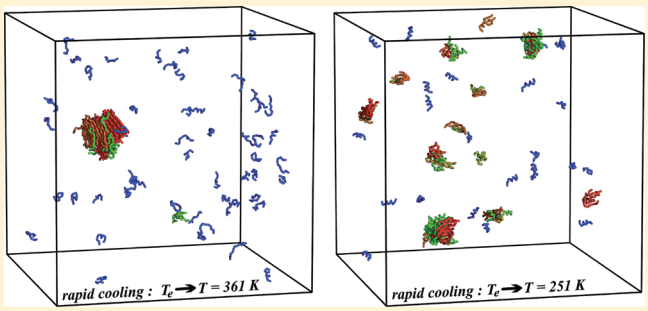

INTRODUCTION

A characteristic feature of proteins is that they can fold into a specific functional structure. During the folding process, or the lifetime of a protein, it can also experience other fates such as assembly into large ordered aggregates known as amyloid fibrils.[1] These aggregates share a common cross-β structure formed by intertwined layers of β-sheets extending in a direction parallel to the fibril axis.[2−4] The ubiquity of this type of assemblies has led to the suggestion that they represent a common structural state of polypeptide chains that is accessible irrespective of the specific amino acid sequences.[5] The question of whether monomeric proteins in their functional native structure are the thermodynamic stable state, or if they are metastable with respect to the amyloid state, is currently the subject of debate.[6] Although this suggestion is not new,[7−9] a recent study by Baldwin et al.[10] provides compelling evidence that, at least for the peptides and proteins studied, the amyloid fibrils can be the most stable structure under physiological conditions. Understanding the thermodynamic stability of proteins under physiological conditions is important because amyloid fibrils are linked to dozens of protein misfolding diseases such as Alzheimer's and Parkinson's.[1]

It is important to keep in mind that when the amyloid phase is thermodynamically most stable, fibrils do not necessarily need to form because the kinetic conditions for fibril formation may not be fulfilled. In fact, the notion that the predictions of a thermodynamic phase diagram are not always realized is not specific to amyloid formation. It has been known for more than a century that liquids can be undercooled or trapped in glass or gel-like states.[11] The actual final state often depends strongly on the starting point in the phase diagram, and discrepancies between predictions and observations are due to the particularities of the hindered kinetics of phase transitions.[12] The questions therefore arise: (i) how important is the kinetics in protein aggregation, and (ii) what properties of proteins do cause this behavior? The objective of this Article is to shed light onto the above questions.

METHODS

Protein Model. In this study, we use a coarse grained model for a polypeptide originally developed by Hoang and co-workers[13] and later adapted by Auer et al. for both Monte Carlo simulations[14] and discontinuous molecular dynamics.[15] The main features of the model are that the amino acids are represented by hard spheres centered on their C_α atoms, and the excluded volume within the chain is treated so as to mimic a semiflexible "tube". The directional H-bonding is sequence-independent and has been tuned to reproduce the geometric arrangements of C_α atoms involved in H-bonding patterns within protein structures listed in the Protein Data Bank.[13] All of the intrachain interactions are modeled by pairwise square-well potentials, while the depth of the hydrogen-bond well, ε, serves as an energy unit. The hydrophobically mediated bonding is assigned an energy gain, ε_h, per hydrophobic (HP-) contact. Steric constraints due to (omitted) side chains are modeled as bending stiffness by applying an energetic penalty, ε_s, when two next-to-adjacent C_α atoms approach each other too close. As in previous studies,[14−17] the relative strength of the H-bonds and HP-contacts is set to $\varepsilon_h/\varepsilon = 0.05$, and the stiffness energy is set to $\varepsilon_s/\varepsilon = 0.3$.

We consider the phase behavior and aggregation kinetics of a simple prototype of biomolecular system consisting of 12-

Received: March 23, 2012
Revised: April 18, 2012
Published: April 18, 2012

ACS Publications © 2012 American Chemical Society

dx.doi.org/10.1021/jp302797c | J. Phys. Chem. B 2012, 116, 5384−5390

residue homopeptides in an implicit aqueous solution. Previous simulations[16,17] showed that most of the peptides in the solution fold at least partially into a native α-helical structure at temperatures below the folding temperature $T_f = 0.2\ \varepsilon/k$, and unfold at least partially into an extended random-coil structure above it (T_f is the temperature at which on average one-half of the intrapeptide hydrogen bonds are formed). Our simulation model is thus pertinent to peptides with hydrogen-bond energy $\varepsilon = (1.9–2.5)\ 10^{-20}$ J, because these ε values correspond to T_f = 276–363 K, that is, to peptide folding temperatures of biophysical relevance. In this study, to obtain a representation of the phase diagram for exemplary, synthetic peptide, we specify the strength of a hydrogen bond $\varepsilon = 2.07 \times 10^{-20}$ J such that the folding temperature of the peptide is T_f = 300 K.

Simulation Method. To describe the kinetics of peptide assembly, we performed discontinuous molecular dynamics (DMD) simulations. The main difference between conventional molecular dynamics simulations and DMD is that the peptide system evolves on a collision by collision basis, and requires the calculation of the collision dynamics and the search for the next collision. The time between collisions is the so-called free flight time and sets the time scale in our simulations. All simulations were performed with 125 (12-residue) homopeptides in the NVT ensemble using an Anderson thermostat. Furthermore, we used a cubic box and applied periodic boundary conditions.

As in previous work,[15] to associate the free flight time in our simulation to a real time, we measured the long time self-diffusion coefficient of our model peptide, D_{Pep} = 1118 Å^2/reduced time unit at T = 300 K, and matched it to experimental data. We took from the literature the value for the self-diffusion coefficient, $D_{Lys} = 13.7 \times 10^{-7}$ cm^2/s, which was measured for lysozyme.[18] The Einstein relation for the diffusion coefficient, together with the Stokes law, yields $D = kT/6\pi\eta r$, where k is the Boltzmann constant, r is the radius of the diffusing object, and η is the viscosity. The latter can be evaluated through kinetic theory as $\eta \propto nkT\tau$, where n is the density of the viscous medium in which diffusion takes place, and τ is the mean flight time between collision with solvent molecules setting the time scale.[19] The resulting expression for the diffusion coefficient $D \propto 1/nr\tau$ allows us to get $\tau_{Lys}/\tau_{Pep} = D_{Pep}r_{Pep}/D_{Lys}r_{Lys} \cong 25.7$ ns as an estimate of the real time corresponding to one free flight time unit in our molecular dynamics simulations. The above value was obtained with r_{Lys} = 19 Å as an estimate of r for lysozyme, and r_{Pep} = 5.85 Å as the average radius of gyration of the peptide as found in our simulations. Hence, a free flight time of 1×10^5 corresponds to 0.257 ms.

RESULTS

Thermodynamics: Peptide Phase Diagram. We first consider the thermodynamics of protein aggregation. In a protein phase diagram, the stability of the various phases is defined by means of solubility at which the bulk protein phase neither grows nor dissolves. In recent work,[16,17] we have obtained the solubility diagram pertaining to the oligomeric and fibrillar phases of natively folded α-helical and β-sheet forming peptides. The peptide model is described in the Methods. A plot of this diagram is depicted in Figure 1 in C,T coordinates, C and T being the actual concentration of monomer peptides and the absolute temperature, respectively. The characteristic feature of this phase diagram is that there exist only two thermodynamically stable peptide phases: the solution of predominantly unfolded peptides (the cyan area) and the

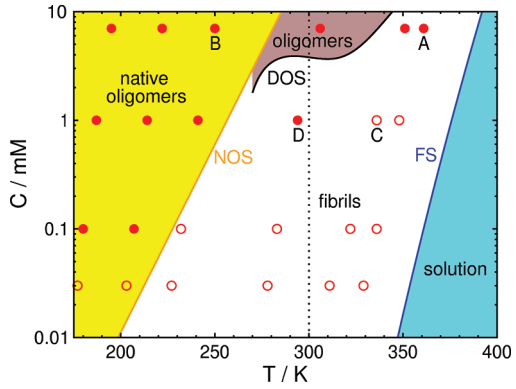

Figure 1. Solubility diagram of α-helical and β-sheet forming peptides. Lines FS, DOS, and NOS are the fibril, disordered oligomer, and native oligomer solubilities, respectively. The labels indicate the regions of solution stability (cyan area), fibril stability (white, brown, and yellow areas), disordered oligomer metastability (brown and yellow areas), and native oligomer metastability (yellow area). The dotted black line indicates the peptide folding temperature T_f. The red open circles indicate the points in the phase diagram at which no aggregation has been observed in the simulations, and the red filled circles indicate points at which aggregation was observed. At point A, the protein solution is supersaturated with respect to the fibrillar phase, because the actual protein concentration C is higher than $C_{e,f}$ at the corresponding temperature T. At point B, the protein solution is supersaturated with respect to both oligomeric phases and the fibrillar phase, because the actual protein concentration C is higher than $C_{e,no}$, $C_{e,do}$, and $C_{e,f}$ at the corresponding temperature T.

fibrillar phase of infinite number of successively layered β-sheets (white area plus the brown and yellow areas). The coexistence line between these two phases is given by the line FS depicting the T dependence of the fibril solubility $C_{e,f}$, that is, the concentration of monomer peptide at which the fibrillar phase is in equilibrium (or coexistence) with the solution. In addition, in the solubility diagram, there exist metastable oligomeric phases (the brown and yellow areas), which are again stable with respect to the solution, but metastable with respect to the fibrillar phase. Lines DOS and NOS in Figure 1 represent the T dependence of the disordered and native oligomer solubilities $C_{e,do}$ and $C_{e,no}$, respectively, that is, the concentration of monomer peptide at which the metastable oligomeric phases and the solution are in thermodynamic equilibrium. Native oligomers are constituted solely of fully folded α-helical peptides, whereas disordered oligomers are composed of fully folded, partially folded, and unfolded peptides. At T values much below T_f, the DOS and NOS lines should merge, because the fraction of fully folded peptides in the solution increases at lower temperatures.

The solution conditions under which fibrils and oligomers can form are now well-defined. At a given C,T pair, fibrils can nucleate if C is in the range $C > C_{e,f}(T)$, whereas both fibrils and disordered or native oligomers can nucleate when $C > C_{e,do}(T)$ or $C > C_{e,no}(T)$. Although the above thermodynamic conditions are a prerequisite for formation of oligomers or fibrils, it is kinetics that decides whether they actually form. The importance of kinetics in peptide aggregation is considered below.

Kinetics: Temperature Effect. We first describe a molecular dynamics simulation (see Methods) performed at a high concentration C = 7 mM. At the beginning of the simulation, a fully equilibrated peptide system was instantly cooled from equilibrium temperature T_e = 390 K to T = 361 K

dx.doi.org/10.1021/jp302797c | J. Phys. Chem. B 2012, 116, 5384–5390

(point A in Figure 1). At this T value, the dimensionless supersaturation s can be calculated and is given by $s = \Delta\mu/kT = 1$ (see Table 1). The sequence of configurations obtained from the simulations is shown in Figure 2a–d and animation 1 (Supporting Information). Analysis of the simulation trajectory depicted in Figure 3 (black circles) shows that initially, during the first ~0.1 ms, a steady-state distribution of small oligomers establishes in the peptide solution. These precritical oligomers constantly form and decay in the solution, and their number fluctuates between $N = 5$ and 17 (Figure 3a, black circles). At this time, the size n of the largest oligomer that forms fluctuates between two and six peptides (Figure 3b, black circles). It is only after a lag time $t \geq 0.1$ ms that one oligomer slowly starts growing and finally reaches a postcritical size of $n = 78$ peptides at the end of the simulation (Figure 3b, black circles, and Figure 2a–d). The largest oligomer grows at the expense of the smaller oligomers whose number decreases and fluctuates between $N = 1$ and 8 (Figure 3a, black circles) at the end of the simulation. This is so, because the simulations are performed at constant volume, and as more and more peptides become part of the largest oligomer, the peptide solution concentration decreases (Figure 3c, black circles), thereby reducing the solution supersaturation s. The structural evolution of the largest oligomer in the solution is described in Figure 3d. As can be seen, initially the oligomer is highly disordered, as both the α-helical content (black circles) and the β-sheet content (brown circles) are low. The α-helical content is defined by the fraction of α-helical hydrogen bonds in the oligomer. It is 1 if all peptides in the oligomer are fully folded, and 0 if all peptides are fully unfolded. Similarly, the β-sheet content is defined by the fraction of peptides in β-sheets. It is 1 if all peptides in the oligomer is part of a β-sheet, and 0 if none. Two peptides form a β-sheet if the number of interpeptide hydrogen bonds between them is larger than 5 (out of the possible 10). The β-

Table 1. List of C,T Pairs At Which Simulations Have Been Performed[a]

$\Delta\mu/kT$	T/K (C = 0.03 mM)	T/K (C = 0.1 mM)	T/K (C = 1 mM)	T/K (C = 7 mM)
0	354	362	375	390
1	329	336	348	361
1.7	311	323	336	351
3	278	284	294	306
5	227	233	242	251
6	202	207	215	222
7	177	180	188	195

[a]At a given T value, the supersaturation is given by $\Delta\mu(T) = (L/T_e)\Delta T$, where $\Delta T = T_e - T$ is the undercooling and T_e is the equilibrium temperature. The latent heat L for the aggregation of a peptide into the infinitely thick β-sheet crystal was determined previously.[16] With a strength of a hydrogen bond $\varepsilon = 2.07 \times 10^{-20}$ J, corresponding to the folding temperature of the peptide $T_f = 300$ K, $L = 14\varepsilon = 2.90 \times 10^{-19}$ J.

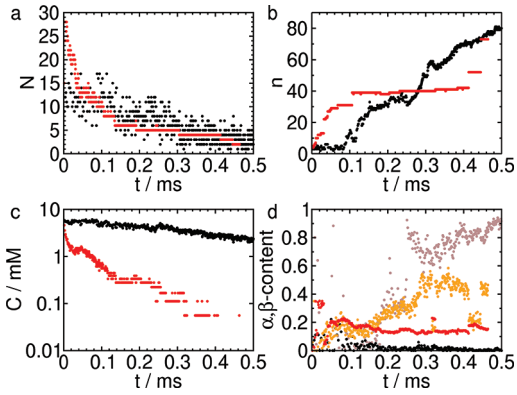

Figure 3. Analysis of the time evolution of the peptide self-assembly process illustrated in Figure 2 at $C = 7$ mM after instant cooling from $T_e = 390$ K to $T = 361$ K (black and brown circles) and $T = 251$ K (red and orange circles). (a) Total number N of oligomers of any size in the peptide solution. (b) Size n of the largest oligomer in the peptide solution. (c) Concentration of peptides in the solution. (d) Structure of largest oligomer in the peptide solution: black and red circles, α-helical content at $T = 361$ K and $T = 251$ K, respectively; brown and orange circles, β-sheet content at $T = 361$ K and $T = 251$ K, respectively.

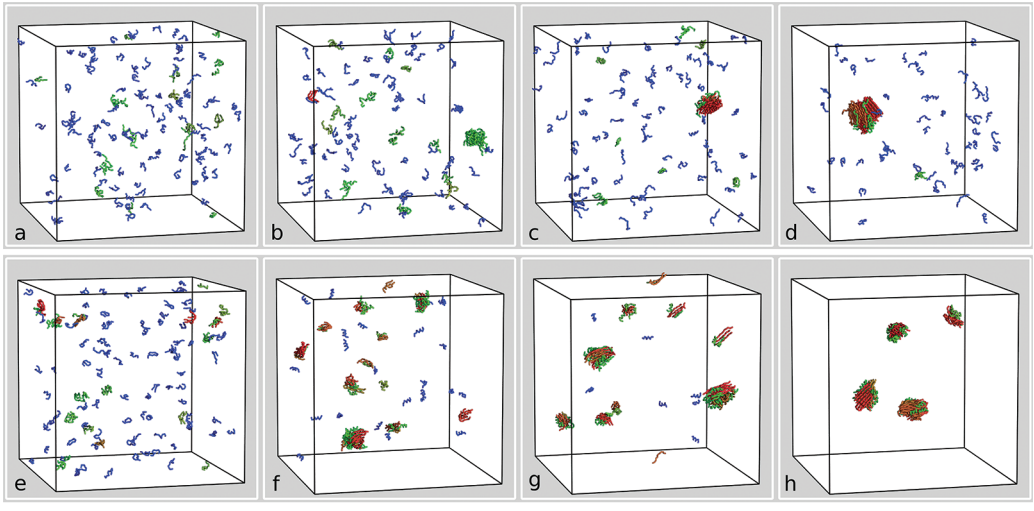

Figure 2. (a–d) Sequence of configurations obtained from the simulations at $C = 7$ mM and $T = 361$ K at times $t = 0.026$, 0.128, 0.257, and 0.385 ms, respectively. (e,f) Sequence of configurations obtained from the simulations at $C = 7$ mM and $T = 251$ K at times $t = 0.016$, 0.051, 0.128, and 0.385 ms, respectively. Peptides in the solution are shown in blue, peptides within an aggregate that do not form interpeptide hydrogen bonds are shown in green, and those that do so are shown in brown or red.

dx.doi.org/10.1021/jp302797c | J. Phys. Chem. B 2012, 116, 5384–5390

sheet content increases at later times, $t > 0.2$ ms, as $n > 30$. At this temperature, the α-helical content of the oligomer is negligible. The described condensation−ordering transition (or nucleated conformational conversion) has been observed in numerous molecular simulations (e.g., refs 14,20−26) and experimental studies (e.g., refs 27−31).

For this C,T pair, only the thermodynamic condition for fibril formation, $C > C_{e,f}(T)$, is fulfilled, whereas the thermodynamic condition for disordered oligomer formation, $C > C_{e,do}(T)$, is not. The observation of rather stable disordered oligomers in the described simulation seems at odds with the phase diagram layout where point A appears to within the area of thermodynamics stable fibrillar aggregates, but outside the region of metastable disordered oligomeric phases (Figure 1, brown area). The reason for this is that in our previous calculation of $C_{e,do}(T)$, it was imposed that a peptide could not form more than one interchain hydrogen bond with any other peptide in the disordered oligomer, so as to prevent spontaneous transformation into fibrils. This restriction implies that $C_{e,do}(T)$ is a lower limit for the disordered oligomer solubility. However, as the β-sheet content within the observed disordered oligomer emerges relatively fast (see Figure 3d), they quickly become less soluble. This explains why the disordered oligomers can already be observed at point A in our simulations. Thermodynamics predicts, however, that at this temperature the fibrillar phase is most stable, which is why it is ecpected, and kinetically observed, that the disordered oligomer transforms into the fibrillar phase.

To illustrate the effect of cooling to much lower temperatures at $C = 7$ mM, we describe a second simulation where a fully equilibrated peptide system was instantly cooled from $T_e = 390$ K to temperature $T = 251$ K (point B in Figure 1). The sequence of configurations obtained from the simulations is shown in Figure 2e−h and animation 2 (Supporting Information). At this high supercooling, corresponding to $s = 5$ (see Table 1), the peptides in the solution quickly aggregate into about $N = 28$ initially small oligomers (Figure 3a, red circles). Several of these oligomers rapidly grow to larger sizes (Figure 2e−h and Figure 3b, red circles). As in the previous simulation, the larger oligomers grow at the expense of the smaller ones, causing the peptide concentration to decrease rapidly (Figure 3c), whereas the number of oligomers reduces to $N = 4$ at the end of the simulation run (Figure 2h). Interestingly, with time, larger oligomers merge, which is revealed by the jumps in the size of the largest oligomer n shown in Figure 3b (red circles). Furthermore, due to the instant temperature drop at the beginning of the simulation, the oligomers retain more disordered structure than that predicted by the phase diagram, as both the α-helical content and the β-sheet content are low (see Figure 3d, red and orange circles, respectively).

In point B, the thermodynamic conditions $C > C_{e,do}(T)$, $C > C_{e,no}(T)$, and $C > C_{e,f}(T)$ for formation of native oligomers, disordered oligomers, and β-sheets, respectively, are all fulfilled. The dominant species observed at the end of the simulation are the disordered oligomer. It is kinetics that prevents the appearance of both native oligomers and fibrils. In this case, rapid oligomerization prevents peptides from folding into their native α-helical structure, and the high supercooling kinetically traps them in only partially structured conformations, which results in delaying or even preventing the formation of the thermodynamically most stable fibrils.

In total, at $C = 7$ mM we performed simulations at six different temperatures instantly cooling a fully equilibrated peptide system from $T_e = 390$ K to $T = 361$, 351, 306, 251, 222, and 195 K. These T values correspond to dimensionless solution supersaturations $s = 1$, 1.7, 3, 5, 6, and 7 (see Table 1). At each T value, we performed 10 independent simulations, and the analysis of the configuration obtained at the end of the simulations is presented in Figure 4 (green ▲). As can be seen

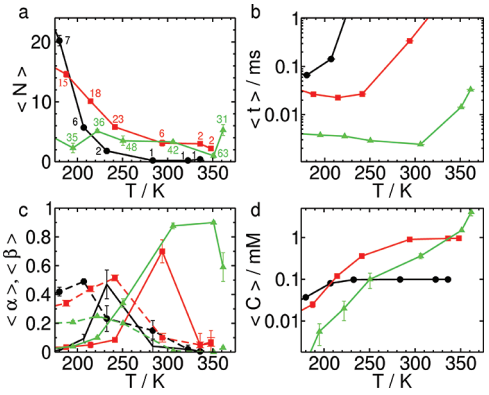

Figure 4. Analysis of the configuration obtained at the end of the simulation run ($t = 0.47$ ms) at $C = 7$ mM (green ▲), $C = 1$ mM (red ■), and $C = 0.1$ mM (●), after instant cooling from T_e to T as indicated by the symbols. (a) Average total number $\langle N \rangle$ of oligomers in the peptide solution. The numbers at the symbols indicate the average size $\langle n \rangle$ of the largest oligomer in the peptide solution. (b) Average time t to form an oligomer of size 10 for $C = 7$ mM and $C = 1$ mM, and size 5 at $C = 0.1$ mM. (c) Structure of the largest oligomer in the peptide solution: dashed line, α-helical content; solid line, β-sheet content. (d) Average solution concentration C. The data shown in this figure have been averaged over 10 independent simulation runs.

from Figure 4a, the average number $\langle N \rangle$ of clusters formed in the solution seems to depend weakly on T, whereas the average size $\langle n \rangle$ of the largest oligomer in the peptide solution goes through a maximum as T decreases. The largest oligomers are formed at $T = 350$ K, and their average size is $\langle n \rangle = 63$ (see Figure 4a, numbers at triangles). The fact that there is an optimal temperature to grow large oligomers is well-known and has already been reported previously.[21,32−34] At high T values, the supersaturation s is simply too low for oligomer formation. At very low T values (large s), the average formation time of at least one oligomer of a certain minimum size is very short (Figure 4b), and several oligomers appear simultaneously. The growth of more than one oligomer in the solution limits their average size. The optimal T corresponds to slow growth of only one oligomer. Analysis of the structure of the largest oligomer obtained at the end of the simulation confirms that at high temperatures the β-sheet content is dominant, whereas at lower T the oligomers become increasingly disordered (Figure 4c). As before, the growth of several large oligomers causes the solution concentration to decrease. The lower are the temperatures, the lower is the peptide concentration in solution (Figure 4d).

Taken together, the simulation results show that the degree of supercooling has two main effects on the correlation between thermodynamics and kinetics. The first is that it determines the structure of the oligomer that is formed, and the second is that it can be used to control the oligomer size.

Kinetics: Concentration Effect. To investigate the concentration effect on the mechanism of peptide aggregation, we next describe our simulations performed at $C = 1$ mM. After

dx.doi.org/10.1021/jp302797c | J. Phys. Chem. B 2012, 116, 5384−5390

equilibration, at T_e = 375 K, the peptide system was instantly cooled to a lower T value at the beginning of the simulation. The chosen T = 348, 336, 294, 242, 215, and 188 K values are such that the supersaturation s = 1, 1.7, 3, 5, 6, and 7 of the peptide solution, respectively, is the same as at C = 7 mM (see Table 1). A sequence of configurations obtained from the simulations at T = 336 K (point C in Figure 1) is shown in animation 3 (Supporting Information). Although small oligomers constantly form and dissolve, the supersaturation s = 1.7 is not high enough for them to grow to postcritical size. Aggregation occurs in the simulations performed at T = 294 K, and a sequence of configurations obtained from the simulations is presented in animation 4 (Supporting Information). As can be seen from the animation, the condensation−ordering transition is much less pronounced than in the simulations performed at higher concentrations (points A and B in Figure 1). The disordered oligomers either do not form, or their lifetime is very short, and the peptides aggregate directly into β-sheets.

The observation that at lower concentration oligomer formation is less favored can be rationalized with help of the phase diagram. At T = 294 K, only the thermodynamic conditions $C > C_{e,f}(T)$ for fibril formation is fulfilled. The main reason why the condensation−ordering transition is less pronounced is that point D in Figure 1 is far away from both the DOS and the NOS solubility lines; that is, the conditions $C > C_{e,do}(T)$ and $C > C_{e,no}(T)$ are not fulfilled.

As previously, for each T value, we performed 10 independent simulations, and a summary of the analysis of all configurations obtained at the end of the simulation run is presented in Figure 4 (red ■). At this concentration, there is a pronounced increase in $\langle N \rangle$ as T decreases, and the maximum for $\langle n \rangle$ is shifted to lower temperatures (Figure 4a, red ■ and numbers). The largest oligomers are formed at T = 242 K, and their average size is $\langle n \rangle$ = 23. Furthermore, the average time it takes to form an oligomer of size n = 10 is increased by 1 order of magnitude (Figure 4b). As a consequence, peptides have more time to fold, and the α-content of the peptides within the oligomer increases at the expense of the β-content (Figure 4c). At very low temperatures, the α-content dominates and the β-content is essentially absent. Here, also it is the kinetics that prevents the appearance of both disordered oligomers and fibrils because the high supercooling traps the peptides kinetically in native oligomer conformations, thereby hindering the formation of the thermodynamically more stable disordered oligomers or fibrils.

The general trends described above, of the effect of reducing the solution concentration on the kinetics of peptide aggregation, are confirmed by the simulation results obtained at C = 0.1 mM (Figure 4, ●). Remarkably, in the simulations performed at C = 0.03 mM, no aggregation was observed at all temperatures ($177 \leq T \leq 354$ K). The main reason for this intriguing behavior is the ability of the peptides to fold into their native α-helical structure. Once folded into the helix, a peptide becomes saturated by intra α-helical hydrogen bonds, and therefore become inactive for aggregation, at least during the simulation time. All C,T pairs at which aggregation was observed in our simulations (red ●) and at which it was not (red ○) are shown in Figure 1.

To summarize, the simulation results show that the concentration has three main effects on the correlation between thermodynamics and kinetics in peptide aggregation. The first is that it determines the structure of the oligomer that is formed, the second is that it can be used to control the oligomer size, and the third is that at low concentrations, no aggregation occurs over the entire temperature range and simulation time studied.

Kinetics: Dependence on Starting Configuration. Finally, we investigated the effect of the starting configuration on the mechanism and structures obtained in peptide aggregation. We repeated all simulations at the C,T pairs listed in Table 1. In contrast to the previous simulations where at the beginning of the simulation a fully equilibrated peptides system was instantly cooled from T_e to the desired T, all simulations were started from a cubic lattice configuration of fully folded helical peptides with different initial velocities assigned at the beginning of the simulations. The main effect of the different starting configuration is that it affects the structure of the oligomers formed in the peptide solution. A comparison of the configurations obtained at the end of the simulations shows that the α-helical content of the oligomer is much more pronounced (Figure 5). Although the starting configuration, for example, the presence of helically folded peptides, affects the structure of the emerging oligomers, aggregation was observed for all C,T pairs as in the instant cooling simulations described above.

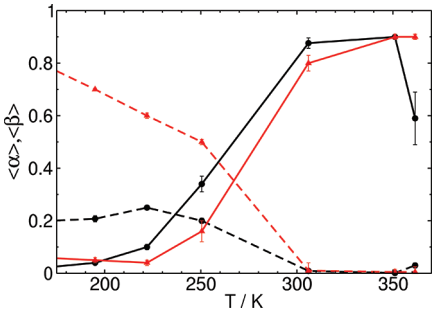

Figure 5. Effect of starting position in the phase diagram on the structure of the largest oligomers in the peptide solution obtained at the end of the simulation run (t = 0.47 ms) at C = 7 mM. Starting position T_e: α-helical content, dashed black line; β-sheet content, solid black line. Starting position T (fully folded α-helix): α-helical content, dashed red line; β-sheet content, solid red line. The data shown in this figure have been averaged over five independent simulation runs.

■ DISCUSSION

The comparison between the thermodynamically predicted and kinetically observed aggregation behavior obtained with natively folded α-helical and β-sheet forming peptides reveals that kinetics is a crucial factor in protein aggregation, in large part determining its aggregation pathways and the morphology of the resulting aggregates. Our simulations shed new light on a number of central questions in the field of protein aggregation, which we discuss below.

Amyloid fibrils have been suggested to nucleate either in one or two steps, but the conditions at which the two mechanisms operate are not clear (see, e.g., refs 27,29,30,35,36). The quantitative calculation of a solubility diagram pertaining to the oligomeric and fibrillar phases of natively folded α-helical and β-sheet forming peptides[16,17] allowed us to define the solution conditions under which fibrils and oligomers can form. At a given C,T pair, fibrils can nucleate if C is in the range $C > C_{e,f}(T)$, whereas both fibrils and disordered or native oligomers can nucleate when $C > C_{e,do}(T)$ or $C > C_{e,no}(T)$. These

dx.doi.org/10.1021/jp302797c | J. Phys. Chem. B 2012, 116, 5384−5390

thermodynamic conditions are a prerequisite for formation of oligomers or fibrils, and here we show that depending on the position in the phase diagram the fibrillar aggregates can form in either one or two steps. Two-step nucleation of fibrils was observed for C,T pairs for which all thermodynamic conditions have been fulfilled (i.e., point B in Figure 1) or when the pair is close to the solubility line (e.g., point A in Figure 1). One-step nucleation of fibrils occurred for C,T values further away from the oligomer solubility lines (i.e., point D in Figure 1). What is important to have in mind is that even when the thermodynamic condition for oligomer formation is fulfilled, fibrils do not necessarily need to form by two steps only. Actually, one-step and two-step nucleation can occur in parallel, but it is solely the strongly dominating process that manifests itself experimentally. Thus, the main reason why, for example, polyglutamine[37] seems to form fibrils in one step, and Aβ_{40} in two steps,[30] can be that either the thermodynamic or the kinetic conditions are not fulfilled.

Structural experiments[29,38−59] show that the oligomeric structure can vary from that of highly disordered aggregates composed of unstructured proteins to that of native-like aggregates in which the proteins retain their native state. At present, a general understanding of the solution conditions needed for the formation of the various oligomeric structures still needs to be developed. The kinetic simulations of the natively folded α-helical and β-sheet forming peptides in combination with the thermodynamic solubility diagram allow us to rationalize the solution conditions for formation of native oligomers, disordered oligomers, and fibrils. Oligomers that form spontaneously at relatively low solution supersaturation easily convert into fibrils. This situation corresponds to on-pathway intermediates that contain β-sheet structure and become increasingly stable during the assembly process.[47,48,53] At higher supersaturations, the structure of the oligomers obtained at the end of the simulation becomes increasingly disordered and have a low α-helical and β-sheet content. It is kinetics that prevents the appearance of both native oligomers and fibrils. The rapid aggregation of monomeric peptides into the oligomers prevents them from folding into their native α-helical structure, and the high supercooling kinetically traps the peptides in disordered conformations, delaying or even preventing the formation of the thermodynamically most stable fibrils. This phenomenon parallels the freezing-in of the disorder of a liquid during rapid undercooling and the resulting vitrification of the liquid. The disordered oligomers that remain in solution also correspond to on-pathway intermediates, some of which have an enhanced cytotoxic potential.[38,42,46,55] In the case of the natively folded α-helical and β-sheet forming peptides, off-pathway intermediates do not exist, because the fibrillar phase is thermodynamically by far the most stable phase. To obtain the experimentally observed native-like oligomers (see, e.g., ref 60), we needed to perform a simulation starting with fully folded peptides.

Perhaps the most interesting finding in our study is that at low concentrations the peptides do not aggregate during the simulation run, despite that the fibrillar phase is by far the thermodynamically most stable one. In fact, the concentration C = 0.03 mM at which the peptides did not aggregate at all temperatures, 177 ≤ T ≤ 354 K, is in the concentration range at which in vitro experiments are commonly performed. The degree of supersaturation (s > 7) achieved for the natively folded α-helical and β-sheet forming peptides is extremely high. The main reason for this intriguing behavior is the ability of the peptides to fold into their native α-helical structure. Once folded, the hydrogen bonds of the peptides are satisfied by intra α-helical hydrogen bonds, and they become inactive for aggregation. This result allows one to rationalize the suggestion[7−10] that monomeric proteins in their native functional structure can be metastable with respect to the amyloid state, and that the native fold is the special property that protects them from aggregation.

CONCLUSIONS

In summary, the results obtained lead to the conclusion that kinetics is very important in protein aggregation. The intrinsic property of proteins to fold into a well-defined native structure allows them to retain a monomeric state even though the fibrillar phase is thermodynamically much more stable. The main reason that prevents the formation of the thermodynamically most stable phase is in contrast to the one observed for undercooled liquids, in which the atoms or molecules are trapped in glass or gel-like states. It is the ability of proteins to switch between an aggregation prone conformation (the unfolded state) to an aggregation immune conformation (the native state). This observation helps one to rationalize the suggestion that monomeric proteins in their native functional structure can be metastable with respect to the amyloid state. The verification of the generic nature of this finding needs more simulations and, more importantly, the experiments[61] that determine both the solubility diagram and the kinetic aggregate structures obtained for different proteins.

ASSOCIATED CONTENT

Supporting Information

Animation 1: The sequence of configurations obtained from molecular dynamics simulations at C = 7 mM. At the beginning of the simulation, a fully equilibrated peptide system was instantly cooled from equilibrium temperature T_e = 390 K to T = 361 K (point A in Figure 1); see also Figure 2a−d. The total simulation time is t = 0.67 ms, and the configurations shown are separated by a time step of Δt = 0.67/100 ms. Animation 2: The sequence of configurations obtained from molecular dynamics simulations at C = 7 mM. At the beginning of the simulation, a fully equilibrated peptide system was instantly cooled from equilibrium temperature T_e = 390 K to T = 251 K (point B in Figure 1); see also Figure 2e−h. The total simulation time is t = 0.46 ms, and the configurations shown are separated by time step of Δt = 0.46/100 ms. Animation 3: The sequence of configurations obtained from molecular dynamics simulations at C = 1 mM. At the beginning of the simulation, a fully equilibrated peptide system was instantly cooled from equilibrium temperature T_e = 375 K to T = 336 K (point C in Figure 1). The total simulation time is t = 1.98 ms, and the configurations shown are separated by a time step of Δt = 1.98/100 ms. Animation 4: The sequence of configurations obtained from molecular dynamics simulations at C = 1 mM. At the beginning of the simulation, a fully equilibrated peptide system was instantly cooled from equilibrium temperature T_e = 375 K to T = 294 K (point D in Figure 1). The total simulation time is t = 1.39 ms, and the configurations shown are separated by a time step of Δt = 1.39/100 ms.

This material is available free of charge via the Internet at http://pubs.acs.org.

dx.doi.org/10.1021/jp302797c | J. Phys. Chem. B 2012, 116, 5384−5390

AUTHOR INFORMATION

Corresponding Author

*E-mail: s.auer@leeds.ac.uk.

Notes

The authors declare no competing financial interest.

ACKNOWLEDGMENTS

We thank Prof. Dimo Kashchiev for stimulating discussions and for his comments on the manuscript. This work was supported by EPSRC grant EP/G026165/1.

REFERENCES

(1) Chiti, F.; Dobson, C. M. *Annu. Rev. Biochem.* **2006**, *75*, 333−366.
(2) Tycko, R. *Q. Rev. Biophys.* **2006**, *39*, 1−55.
(3) Makin, O. S.; Atkins, E.; Sikorski, P.; Johansson, J.; Serpell, L. C. *Proc. Natl. Acad. Sci. U.S.A.* **2005**, *102*, 315−320.
(4) Sawaya, M. R.; Sambashivan, S.; Nelson, R.; Ivanova, M. I.; Sievers, S. A.; Apostol, M. I.; Thompson, M. J.; Balbirnie, M.; Wiltzius, J. J.; McFarlane, H. T.; et al. *Nature* **2007**, *447*, 453−457.
(5) Dobson, C. M. *Trends Biochem. Sci.* **1999**, *24*, 329−332.
(6) Thirumalai, D.; Reddy, G. *Nat. Chem.* **2011**, *3*, 910−911.
(7) Honeycutt, J. D.; Thirumalai, D. *Proc. Natl. Acad. Sci. U.S.A.* **1990**, *87*, 3526−3529.
(8) Dinner, A. R.; Karplus, M. *Nat. Struct. Biol.* **1998**, *5*, 236−241.
(9) Thirumalai, D.; Klimov, D. K.; Dima, R. I. *Curr. Opin. Struct. Biol.* **2003**, *13*, 146−149.
(10) Baldwin, A. J.; Knowles, T. P. J.; Tartaglia, G. G.; Fitzpatrick, A. W.; Devlin, G. L.; Shammas, S. L.; Waudby, C. A.; Mossuto, M. F.; Meehan, S.; Gras, S. L.; et al. *J. Am. Chem. Soc.* **2011**, *133*, 14160−14163.
(11) Debenedetti, P. G.; Stillinger, F. H. *Nature* **2001**, *410*, 259−267.
(12) Anderson, V. J.; Lekkerkerker, H. N. W. *Nature* **2002**, *416*, 811−815.
(13) Hoang, T. X.; Trovato, A.; Seno, F.; Banavar, J. R.; Maritan, A. *Proc. Natl. Acad. Sci. U.S.A.* **2004**, *101*, 7960−7964.
(14) Auer, S.; Dobson, C. M.; Vendruscolo, M. *HFSP J.* **2007**, *1*, 137−146.
(15) Auer, S.; Trovato, A.; Vendruscolo, M. *PLoS Comput. Biol.* **2009**, *5*, e1000458.
(16) Auer, S. *J. Chem. Phys.* **2011**, *135*, 175103.
(17) Auer, S.; Kashchiev, D. *Phys. Rev. Lett.* **2010**, *104*, 168105.
(18) Mattisson, C.; Roger, P.; Jonsson, B.; Axelsson, A.; Zacchi, G. *J. Chromatogr., B* **2000**, *743*, 151−167.
(19) Chaikin, P. M.; Lubensky, T. C. *Principles of Condensed Matter Physics*; Cambridge University Press: Cambridge, 1995.
(20) Auer, S.; Meersman, F.; Dobson, C. M.; Vendruscolo, M. *PLoS Comput. Biol.* **2008**, *4*, e1000222.
(21) Cheon, M.; Chang, I.; Hall, C. K. *Biophys. J.* **2011**, *101*, 2493−2501.
(22) Cheon, M.; Chang, I.; Mohanty, S.; Luheshi, L. M.; Dobson, C. M.; Vendruscolo, M.; Favrin, G. *PLoS Comput. Biol.* **2007**, *3*, e173.
(23) Li, M. S.; Klimov, D. K.; Straub, J. E.; Thirumalai, D. *J. Chem. Phys.* **2008**, *129*, 175101.
(24) Bellesia, G.; Shea, J. E. *J. Chem. Phys.* **2009**, *130*, 145103.
(25) Pellarin, R.; Guarnera, E.; Caflisch, A. *J. Mol. Biol.* **2007**, *374*, 917−924.
(26) Wu, C.; Shea, J. E. *Curr. Opin. Struct. Biol.* **2011**, *21*, 209−220.
(27) Lomakin, A.; Chung, D. S.; Benedek, G. B.; Kirschner, D. A.; Teplow, D. B. *Proc. Natl. Acad. Sci. U.S.A.* **1996**, *93*, 1125−1129.
(28) Lomakin, A.; Teplow, D. B.; Kirschner, D. A.; Benedek, G. B. *Proc. Natl. Acad. Sci. U.S.A.* **1997**, *94*, 7942−7947.
(29) Serio, T. R.; Cashikar, A. G.; Kowal, A. S.; Sawicki, G. J.; Moslehi, J. J.; Serpell, L.; Arnsdorf, M. F.; Lindquist, S. L. *Science* **2000**, *289*, 1317−1321.
(30) Lee, J.; Culyba, E. K.; Powers, E. T.; Kelly, J. W. *Nat. Chem. Biol.* **2011**, *7*, 602−609.
(31) Eichner, T.; Radford, S. E. *Mol. Cell* **2011**, *43*, 8−18.
(32) Nguyen, H. D.; Hall, C. K. *J. Biol. Chem.* **2005**, *280*, 9074−9082.
(33) Nguyen, H. D.; Hall, C. K. *J. Am. Chem. Soc.* **2006**, *128*, 1890−1901.
(34) Zhang, J.; Muthukumar, M. *J. Chem. Phys.* **2009**, *130*, 035102.
(35) Jarrett, J. T.; Lansbury, P. T., Jr. *Cell* **1993**, *73*, 1055−1058.
(36) Schmit, J. D.; Ghosh, K.; Dill, K. *Biophys. J.* **2011**, *100*, 450−458.
(37) Bhattacharyya, A. M.; Thakur, A. K.; Wetzel, R. *Proc. Natl. Acad. Sci. U.S.A.* **2005**, *102*, 15400−15405.
(38) Ahmed, M.; Davis, J.; Aucoin, D.; Sato, T.; Ahuja, S.; Aimoto, S.; Elliott, J. I.; Van Nostrand, W. E.; Smith, S. O. *Nat. Struct. Mol. Biol.* **2010**, *17*, 561−567.
(39) Bernstein, S. L.; Dupuis, N. F.; Lazo, N. D.; Wyttenbach, T.; Condron, M. M.; Bitan, G.; Teplow, D. B.; Shea, J. E.; Ruotolo, B. T.; Robinson, C. V.; Bowers, M. T. *Nat. Chem.* **2009**, *1*, 326−331.
(40) Calabrese, M. F.; Eakin, C. M.; Wang, J. M.; Miranker, A. D. *Nat. Struct. Mol. Biol.* **2008**, *15*, 965−971.
(41) Calamai, M.; Canale, C.; Relini, A.; Stefani, M.; Chiti, F.; Dobson, C. M. *J. Mol. Biol.* **2005**, *346*, 603−616.
(42) Chimon, S.; Shaibat, M. A.; Jones, C. R.; Calero, D. C.; Aizezi, B.; Ishii, Y. *Nat. Struct. Mol. Biol.* **2007**, 1157−1164.
(43) Dusa, A.; Kaylor, J.; Edridge, S.; Bodner, N.; Hong, D. P.; Fink, A. L. *Biochemistry* **2006**, *45*, 2752−2760.
(44) Knaus, K. J.; Morillas, M.; Swietnicki, W.; Malone, M.; Surewicz, W. K.; Yee, V. C. *Nat. Struct. Biol.* **2001**, *8*, 770−774.
(45) Kokubo, H.; Kayed, R.; Glabe, C. G.; Staufenbiel, M.; Saido, T. C.; Iwata, N.; Yamaguchi, H. *Int. J. Alzheimer's Dis.* **2009**, *2009*, 689285.
(46) Lashuel, H. A.; Petre, B. M.; Wall, J.; Simon, M.; Nowak, R. J.; Walz, T.; Lansbury, P. T., Jr. *J. Mol. Biol.* **2002**, *322*, 1089−1102.
(47) Oliveira, C. L.; Behrens, M. A.; Pedersen, J. S.; Erlacher, K.; Otzen, D. *J. Mol. Biol.* **2009**, *387*, 147−161.
(48) Orte, A.; Birkett, N. R.; Clarke, R. W.; Devlin, G. L.; Dobson, C. M.; Klenerman, D. *Proc. Natl. Acad. Sci. U.S.A.* **2008**, *105*, 14424−14429.
(49) Pieri, L.; Bucciantini, M.; Nosi, D.; Formigli, L.; Savistchenko, J.; Melki, R.; Stefani, M. *J. Biol. Chem.* **2006**, *281*, 15337−15344.
(50) Plakoutsi, G.; Bemporad, F.; Monti, M.; Pagnozzi, D.; Pucci, P.; Chiti, F. *Structure* **2006**, *14*, 993−1001.
(51) Poirier, M. A.; Li, H.; Macosko, J.; Cai, S.; Amzel, M.; Ross, C. A. *J. Biol. Chem.* **2002**, *277*, 41032−41037.
(52) Relini, A.; Torrassa, S.; Rolandi, R.; Gliozzi, A.; Rosano, C.; Canale, C.; Bolognesi, M.; Plakoutsi, G.; Bucciantini, M.; Chiti, F.; Stefani, M. *J. Mol. Biol.* **2004**, *338*, 943−957.
(53) Smith, D. P.; Radford, S. E.; Ashcroft, A. E. *Proc. Natl. Acad. Sci. U.S.A.* **2010**, *107*, 6794−6798.
(54) Sorgjerd, K.; Klingstedt, T.; Lindgren, M.; Kagedal, K.; Hammarstrom, P. *Biochem. Biophys. Res. Commun.* **2008**, *377*, 1072−1078.
(55) Wahlbom, M.; Wang, X.; Lindstrom, V.; Carlemalm, E.; Jaskolski, M.; Grubb, A. *J. Biol. Chem.* **2007**, *282*, 18318−18326.
(56) Walsh, P.; Neudecker, P.; Sharpe, S. *J. Am. Chem. Soc.* **2010**, *132*, 7684−7695.
(57) Weise, K.; Radovan, D.; Gohlke, A.; Opitz, N.; Winter, R. *ChemBioChem* **2010**, *11*, 1280−1290.
(58) Wu, J. W.; Breydo, L.; Isas, J. M.; Lee, J.; Kuznetsov, Y. G.; Langen, R.; Glabe, C. *J. Biol. Chem.* **2010**, *285*, 6071−6079.
(59) Zhao, J.; Yu, X.; Liang, G.; Zheng, J. *Biomacromolecules* **2011**, *12*, 210−220.
(60) Chiti, F.; Dobson, C. M. *Nat. Chem. Biol.* **2009**, *5*, 15−22.
(61) Wetzel, R. *Acc. Chem. Res.* **2006**, *39*, 671−679.